SPECTROSCOPIC CCD SURVEYS FOR QUASARS AT LARGE REDSHIFT. IV. EVOLUTION OF THE LUMINOSITY FUNCTION FROM QUASARS DETECTED BY THEIR LYMAN-ALPHA EMISSION

MAARTEN SCHMIDT

Palomar Observatory, California Institute of Technology, Pasadena, California 91125
Electronic mail: mxs@deimos.caltech.edu

DONALD P. SCHNEIDER[1]

Department of Astronomy and Astrophysics, The Pennsylvania State University, University Park, Pennsylvania 16802, and Institute for Advanced Study, Princeton, New Jersey 08540
Electronic mail: dps@astro.psu.edu

JAMES E. GUNN[2]

Princeton University Observatory, Princeton, New Jersey 08544
Electronic mail: jeg@astro.princeton.edu

Received 1995 January 19; revised 1995 March 7

ABSTRACT

We use 90 quasars detected by their Lyα emission to well-defined flux limits in the Palomar Transit Grism Survey to derive the luminosity function of quasars in the redshift range 2.75–4.75. Application of the $V/V_{\max}$ test yields $\langle V_e/V_a\rangle = 0.377 \pm 0.026$, corresponding to a nonuniform distribution in comoving coordinates, such that the space density decreases with redshift. The luminosity function appears to be well represented by a power law with a slope corresponding to a factor of 5.6 per magnitude. We discuss and define the relationship between the line luminosity function and the continuum luminosity function of quasars. The space density for $M_B < -26$ decreases by a factor of 2.7 per unit redshift beyond $z = 2.7$. Based on this result and earlier published work on quasar luminosity functions at lower redshifts, it appears that there is a maximum in the comoving space density of quasars with $M_B < -26$ between redshifts 1.7 and 2.7.

1. INTRODUCTION

The existence of quasars with redshifts $z > 4$ is important for our understanding of the formation of galaxies and of quasars themselves (cf. Efstathiou & Rees 1988; Turner 1991; Haehnelt & Rees 1993; Loeb 1993; Katz *et al.* 1994). In this paper, we show that the luminosity function of quasars of average luminosity exhibits a sharp peak at a redshift between 1.7 and 2.7, showing that the bulk of quasar formation must have occurred at the corresponding epoch.

Soon after the discovery of the redshifts of quasars, it was found that their luminosity function evolves strongly, first for radio selected quasars (Schmidt 1968) and then for optically selected ones (Schmidt 1970). The Palomar Bright Quasar Survey (Schmidt & Green 1983) showed that the increase of comoving space density at given luminosity with redshift was luminosity dependent. Large and deep surveys of optically selected quasars such as the CFHT survey (Crampton *et al.* 1987) and the survey of Boyle *et al.* (1988) allowed a much more detailed study of the evolution of the luminosity function. Boyle *et al.* (1988) derived the luminosity functions at different redshifts below $z = 2.2$. Their compilation showed that the shapes of all the luminosity functions were the same, but that they were shifted in luminosity as a function of redshift, approximately as $(1+z)^{3.2}$. Recently, results from the Large Bright Quasar Survey (LBQS, cf. Morris *et al.* 1991) have been discussed by Hewett *et al.* (1993). Their luminosity functions for $z < 2$ show that the shape changes with redshift.

For redshifts larger than 2.2, many quasars do not show an ultraviolet excess because the Lyα emission line appears at wavelengths redward of the U filter response, and the continuum below Lyα is depressed by the Lyα forest. Most searches for these quasars are conducted on the basis of multicolor or grism observations. Early grism searches for quasars at high redshift, based on the detection of the Lyα emission line in the low-dispersion grism spectra, were very successful (cf. the review by Smith 1983). However, the completeness of these surveys became a concern when Osmer (1980) found that surface densities on the sky depended strongly on the plate scale of the survey instrument. Osmer (1982) found evidence for a lack of quasars with redshifts $z > 3.5$ compared to those at $z = 2$, making the study of these high redshift objects a subject of great interest.

Our work, reported in previous papers of this series, has been based on a precise definition of the selection criteria in advance, so that the sample completeness is well defined. Initially, we made CCD observations through a grism of individual fields and were unsuccessful in finding quasars with $z > 2.7$ (Schmidt *et al.* 1986a; hereafter referred to as Paper

[1]Guest Investigator, Palomar Observatory, California Institute of Technology.
[2]Visiting Associate, Palomar Observatory, California Institute of Technology.

 0004-6256/95/110(1)/68/10/$0.90

I). We then turned to transit observations which allowed the study of larger areas, though with shorter exposure times. The initial attempt (Schmidt *et al.* 1986b; hereafter referred to as Paper II) also did not produce high redshift quasars.

The present paper is based on the 90 quasars detected through their Lyα emission in the Palomar Transit Grism Survey (PTGS; Schneider *et al.* 1994; hereafter referred to as Paper III). Slit spectra of many of the objects have been presented in some detail (Schmidt *et al.* 1987a, 1987b; Schneider *et al.* 1989a, 1989b, 1991). In the next section, we derive properties of these quasars needed for the statistical analysis. We discuss in Sec. 3 how a luminosity function based on Lyα luminosities can be converted to one of continuum luminosities or absolute magnitudes. In Sec. 4, we derive the luminosity function. First, we show on the basis of the $V/V_{\rm max}$ test that the comoving density of the quasars at given luminosity decreases with redshift. We then derive the slope of the luminosity function and the comoving density for $M_B<-26$ as a function of redshift. We compare our results with those of multicolor surveys (Warren *et al.* 1994; Irwin *et al.* 1991) in Sec. 5.

2. PROPERTIES OF LYMAN-ALPHA QUASARS IN THE PTGS

Our sample consists of the 90 quasars detected through their Lyα emission in the Palomar Transit Grism Survey (PTGS; Paper III) with redshifts in the range 2.75–4.75. In this section, we discuss the observed and absolute properties of these quasars, in particular their Lyα equivalent widths, line fluxes, and line luminosities, and their absolute magnitudes M_B. The properties of the 90 quasars used in this study are given in Table 1. The table lists the object name, the subsurvey (S) that includes the object (see Paper III), the redshift of the object as determined from the grism spectra, the logarithm of the Lyα line flux (erg cm^{-2} s^{-1}) and the Lyα line luminosity (erg s^{-1}), the AB_{1450} magnitude, the absolute magnitude M_B, and the rest frame equivalent width (in Å) of the Lyα line.

Throughout the paper, we use $H_0=50$ km s^{-1} Mpc^{-1} and $q_0=1/2$. In this case, the bolometric luminosity distance is $(c/H_0)\,A(z)$, where

$$A(z)=2(1+z-\sqrt{1+z}), \tag{1}$$

and the comoving volume to redshift z is

$$V(z)=(32\pi/3)(c/H_0)^3(1-1/\sqrt{1+z})^3. \tag{2}$$

The PTGS gives for each object the following quantities of interest: the redshift z derived from a slit spectrum, the detected line flux f (in erg cm^{-2} s^{-1}), the signal-to-noise ratio (SNR) of the line detection, the observed equivalent width W (in Å), and the linewidth w_0 (in Å). For the analysis discussed in this paper, we have used the redshifts as derived from the grism spectra, cf. Table 1. A histogram of the redshifts is shown in Fig. 1(a).

2.1 Lyα Linewidths, Fluxes, and Luminosities

The line fluxes f listed in Paper III (Table 5, column 5) for the 90 quasars with $z>2.7$ are detected grism fluxes $f_{\rm Ly\alpha,det}$ based on an extraction algorithm assuming a FWHM of 118 Å. Most of the quasars had larger linewidths and therefore the total line flux is larger than the detected flux; the exact value of this ratio depends on the seeing. Table 4 of Paper III gives for each of the six survey fields the ratio R_w of the detected to total line flux as a function of the linewidth w_0. The linewidth at zero redshift $w_{\rm rest}$ is

$$w_{\rm rest}=w_0/(1+z). \tag{3}$$

The total Lyα line fluxes,

$$f_{\rm Ly\alpha}=f_{\rm Ly\alpha,det}/R_w, \tag{4}$$

for the sample of 90 quasars are given in Table 1. We also give the Lyα line luminosities, in erg s^{-1},

$$\log L_{\rm Ly\alpha}=\log f_{\rm Ly\alpha}+2\,\log A(z)+57.633. \tag{5}$$

A histogram of $\log L_{\rm Ly\alpha}$ is shown in Fig. 1(b).

2.2 Absolute Magnitudes M_B

Luminosity functions of quasars with $z<2.2$ have usually been discussed in terms of absolute magnitude M_B (cf. Boyle *et al.* 1988). In order to allow comparisons with other luminosity functions, we will besides the Lyα line luminosities also employ M_B. In making the transformation, we use the AB magnitude system as defined by Oke (1974),

$$AB(\lambda)=-2.5\,\log f_\nu(\lambda)-48.60. \tag{6a}$$

The corresponding absolute magnitude is

$$M_{AB}(\lambda)=-2.5\,\log\left(\frac{L_\nu(\lambda)}{4\pi(10\ \text{pc})^2}\right)-48.60. \tag{6b}$$

Generally, let us assume that a continuum flux density or AB magnitude at a wavelength $\lambda_{\rm obs}$ is observed or can be derived from a broadband magnitude centered on that wavelength (see below). The flux $f_\nu(\lambda_{\rm obs},z)$ for a quasar at redshift z observed over the frequency band $d\nu_{\rm obs}$ is related to the luminosity by

$$f_\nu(\lambda_{\rm obs})d\nu_{\rm obs}=\frac{L_\nu(\lambda_{\rm rest})}{4\pi(A(z)c/H_0)^2}\,d\nu_{\rm rest}, \tag{7}$$

where $\lambda_{\rm rest}=\lambda_{\rm obs}/(1+z)$ and $d\nu_{\rm rest}=(1+z)d\nu_{\rm obs}$. Combining Eqs. (6a), (6b), and (7), we obtain

$$M_{AB}(\lambda_{\rm obs}/(1+z))=AB(\lambda_{\rm obs})-5\,\log A(z)+2.5\,\log(1+z)-43.89. \tag{8}$$

The absolute magnitude so derived does *not* depend on the spectral index α, since it refers to the same rest frame wavelength as the observed magnitude or flux density.

We now assume that the quasar continua have a power law spectrum,

$$f_\nu\sim\nu^\alpha. \tag{9}$$

The absolute AB magnitude at 4400 Å is obtained from that at $\lambda_{\rm obs}/(1+z)$ through Eqs. (6a) and (9),

$$M_{AB}(4400)=M_{AB}(\lambda_{\rm obs}/(1+z))-2.5\alpha\,\log\left(\frac{\lambda_{\rm obs}/(1+z)}{4400}\right). \tag{10}$$

TABLE 1. Properties of Lyman α PTGS quasars.[a]

Object	S	z_{grism}	log f	log L	AB_{1450}	M_B	W_0 Å	Object	S	z_{grism}	log f	log L	AB_{1450}	M_B	W_0 Å
0041+0215	O	2.81	−13.48	45.29	19.50	−26.27	117	1257+3754	K	3.26	−13.71	45.21	19.46	−26.55	75
0047+0121	G	3.07	−13.73	45.13	19.65	−26.26	82	1301+4747	Q	4.00	−14.21	44.91	21.63	−24.71	204
0049+0121	G	3.45	−13.87	45.11	18.93	−27.17	33	1307+4747	Q	2.99	−13.63	45.20	18.98	−26.89	54
0056+0125	H	3.19	−13.27	45.63	18.59	−27.39	92	1308+4749	Q	3.58	−14.24	44.77	21.35	−24.81	135
0103+0123	H	3.07	−13.56	45.30	19.59	−26.32	114	1314+4748A	Q	3.37	−14.07	44.88	19.80	−26.26	46
0104+0215	O	4.15	−13.95	45.20	19.42	−26.97	50	1314+4748B	Q	3.33	−14.15	44.79	21.39	−24.65	165
0118+0119	G	3.26	−13.83	45.08	19.18	−26.83	43	1319+4636	M	3.16	−13.94	44.95	20.20	−25.76	85
0126+0214	O	2.81	−13.50	45.27	20.41	−25.36	259	1321+4752	R	3.16	−13.87	45.02	20.75	−25.21	167
0131+0120	G	3.83	−13.66	45.41	18.93	−27.34	58	1341+3757	L	3.07	−13.58	45.28	19.53	−26.38	104
0234+0120	G	3.32	−13.71	45.23	20.00	−26.04	126	1347+4750	Q	3.37	−14.08	44.87	20.44	−25.62	82
0249+0222	P	2.81	−13.50	45.27	18.45	−27.32	42	1358+4751	R	3.11	−14.04	44.83	20.92	−25.02	129
0307+0222	P	4.40	−13.96	45.25	20.55	−25.94	146	1407+4640	N	3.16	−14.18	44.71	20.41	−25.55	60
0344+0222	O	3.45	−13.91	45.07	20.45	−25.65	124	1414+4746	Q	3.45	−13.73	45.25	19.46	−26.64	75
0345+0130	H	3.70	−13.85	45.19	19.70	−26.51	75	1418+4753	R	2.86	−13.71	45.08	19.89	−25.91	100
0748+5624	J	3.07	−13.67	45.19	19.54	−26.37	85	1430+4635	M	3.37	−13.86	45.09	20.18	−25.88	105
0751+5623	J	4.34	−13.93	45.27	20.17	−26.29	109	1447+4750	R	2.99	−13.65	45.18	19.26	−26.61	66
0852+5621	I	3.00	−13.75	45.08	19.30	−26.58	55	1510+4631	M	3.24	−13.98	44.93	20.49	−25.51	103
0856+4750	R	3.88	−14.17	44.92	20.68	−25.61	91	1519+4743	Q	2.78	−13.46	45.30	18.91	−26.84	71
0902+4750	R	3.07	−13.92	44.94	20.51	−25.41	116	1527+4748	R	3.07	−13.68	45.18	18.90	−27.02	46
0910+5625	J	4.08	−14.28	44.86	20.70	−25.67	75	1529+4632	M	3.45	−13.80	45.18	19.94	−26.16	100
0928+4637	N	3.62	−13.82	45.20	19.45	−26.73	63	1539+4746	Q	3.16	−13.31	45.58	18.58	−27.38	82
0930+4640	N	3.07	−14.08	44.78	19.90	−26.02	46	1542+4744	Q	3.37	−13.48	45.47	18.88	−27.18	76
0947+5628	J	2.94	−13.82	44.99	19.49	−26.35	55	1545+4633	M	2.86	−13.71	45.08	19.95	−25.85	107
0951+4637A	N	3.20	−14.15	44.75	20.89	−25.09	99	1548+4637	N	3.62	−13.72	45.31	19.15	−27.03	60
0951+4637B	N	3.24	−13.74	45.17	19.17	−26.83	53	1601+4636	N	2.82	−13.85	44.93	20.02	−25.75	81
0953+4749	Q	4.56	−13.65	45.60	19.46	−27.08	113	1601+3754	L	3.19	−13.61	45.29	20.00	−25.98	154
0958+5625	I	3.19	−13.96	44.93	20.10	−25.88	74	1605+4631	M	3.28	−13.91	45.02	19.70	−26.32	59
0958+4638	N	3.11	−13.76	45.12	19.85	−26.09	93	1612+4741	Q	3.50	−13.91	45.07	20.12	−26.00	91
1000+4751	R	2.94	−13.67	45.15	20.04	−25.81	130	1619+4631	M	3.50	−13.85	45.13	20.30	−25.82	124
1009+4635	M	3.20	−14.03	44.87	20.66	−25.32	108	1620+4747	R	3.07	−13.67	45.19	19.49	−26.43	81
1010+5630	J	3.70	−13.94	45.10	18.76	−27.45	25	1627+4744	Q	3.11	−13.86	45.02	19.79	−26.15	70
1015+4752	R	2.94	−13.76	45.05	19.40	−26.45	58	1640+4628	M	3.71	−14.16	44.89	19.45	−26.77	29
1027+4635	M	3.11	−14.03	44.84	20.64	−25.30	102	1643+4631A	N	3.83	−13.94	45.13	19.83	−26.44	70
1033+4750	Q	3.67	−14.15	44.89	21.22	−24.98	152	1643+4631B	M	3.88	−14.26	44.83	20.55	−25.74	66
1035+4747	Q	2.94	−13.82	45.00	19.57	−26.28	59	1644+4744	R	3.75	−14.05	45.01	20.60	−25.64	109
1109+4642	N	3.37	−13.42	45.53	18.78	−27.28	81	2047+0123	G	3.83	−14.01	45.06	19.45	−26.82	42
1117+4638	M	3.58	−13.66	45.35	19.67	−26.49	111	2048+0126	H	3.26	−13.91	45.01	20.00	−26.01	78
1125+4753	R	2.86	−13.90	44.89	19.29	−26.51	37	2132+0126	H	3.19	−13.56	45.34	19.68	−26.30	128
1153+4751	Q	3.33	−14.15	44.79	21.69	−24.35	214	2204+0127	H	2.75	−13.61	45.14	19.05	−26.68	57
1158+4635	M	4.72	−13.94	45.34	19.89	−26.71	89	2211+0119	G	3.07	−13.51	45.35	19.06	−26.85	79
1215+4754	R	3.62	−14.14	44.88	20.54	−25.64	81	2226+0216	O	3.26	−13.58	45.34	19.13	−26.88	75
1222+4752	R	3.20	−13.94	44.96	20.13	−25.85	80	2318+0119	G	3.26	−13.71	45.21	18.70	−27.31	37
1233+4752	R	4.51	−14.09	45.15	20.34	−26.19	91	2330+0125	H	3.32	−13.82	45.11	19.56	−26.48	64
1234+4642	N	3.03	−13.53	45.31	19.41	−26.48	102	2331+0216	O	4.15	−13.98	45.17	20.15	−26.24	91
1250+4747	Q	3.20	−13.82	45.08	20.15	−25.83	109	2344+0124	H	3.19	−13.81	45.09	19.12	−26.86	43

[a] See text for a description of the columns.

The offset between $AB(4400)$ and the B magnitude depends slightly on the energy distribution of the source. Convolution of the B-filter system response with an $\alpha=-0.5$ power law spectrum yields an offset of +0.12 mag, so

$$M_B=M_{AB}(4400)+0.12. \tag{11}$$

(The offset of +0.24 given in Schmidt & Green [1983; cf. Eq. (2)] for an $\alpha=-0.5$ power law is incorrect.) Our adopted value is close to the value used by Warren *et al.* (1994). Combining Eqs. (8), (10), and (11), we obtain

$$M_B=AB(\lambda_{obs})-5\log A(z)+2.5\log(1+z)$$
$$-2.5\alpha\log\left(\frac{\lambda_{obs}/(1+z)}{4400}\right)-43.77. \tag{12}$$

We have measured in the grism spectra the continuum flux densities at observed wavelength $1450(1+z)$ Å and derived the corresponding $AB(1450(1+z))$ magnitudes [cf. Eq. 6(a)], usually denoted as AB_{1450}. With $\lambda_{obs}=1450(1+z)$, we get from Eq. (12),

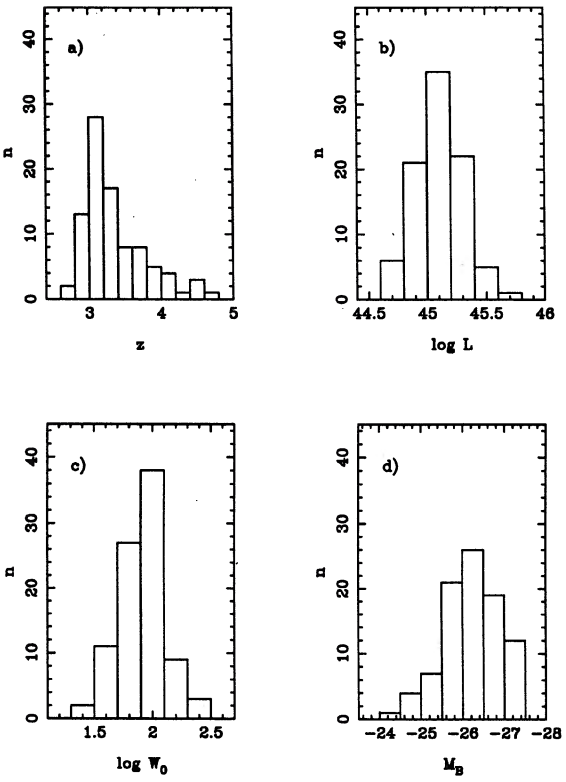

FIG. 1. Histograms of (a) redshifts, (b) luminosities $\log L_{Ly\alpha}$, (c) equivalent widths $\log W_0$, and (d) absolute magnitudes M_B of the 90 Lyα selected quasars in the PTGS.

$$M_B = AB_{1450} - 5\log A(z) + 2.5\log(1+z) + 1.205\alpha - 43.77. \quad (13)$$

The M_B absolute magnitudes for all quasars are given in Table 1; the distribution is shown in Fig. 1(d).

2.3 Rest Frame Equivalent Widths

Due to the strong absorption in the Lyα forest, the continuum at low spectral dispersion shows a large drop from the red side to the blue side of the Lyα emission line. As a consequence, the continuum flux at the observed wavelength of Lyα was poorly determined in the grism spectra, and so was the observed equivalent width W for Lyα listed in the PTGS (Paper III, Table 5).

We can improve the derivation of the continuum under Lyα by using the more accurately determined continuum to the red of the Lyα emission, characterized by AB_{1450}, and extrapolating to the Lyα wavelength. The "red-side" continuum flux density $f_\nu(1216(1+z))$ is obtained from $f_\nu(1450(1+z))$ using Eq. (9). Then, the red-side equivalent width W_0 of the Lyα emission, expressed in Å in the rest frame is

$$W_0 = \frac{f_{Ly\alpha}}{f_\nu(1216(1+z))}\frac{1216^2(1+z)^2}{c}\frac{1}{1+z}. \quad (14)$$

The first term is the observed equivalent width of Lyα into wavelength units, and the last term reduces it to the rest frame. In terms of Ångstroms and the AB_{1450} magnitude, the rest frame equivalent width of the Lyα emission is

$$\log W_0 = \log f_{Ly\alpha} + 0.4AB_{1450} + \log(1+z) - 0.076\alpha + 7.133. \quad (15)$$

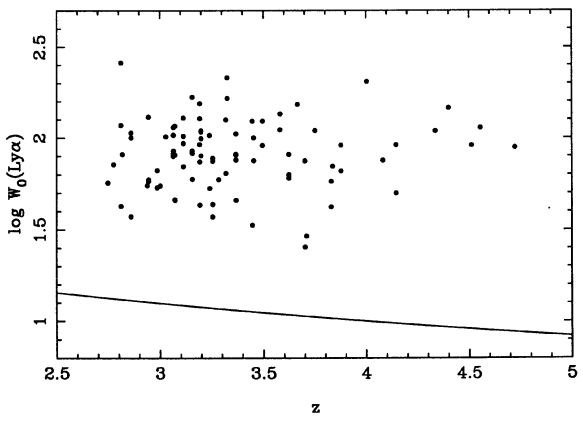

FIG. 2. Rest frame Lyα equivalent widths versus redshift for the 90 quasars detected by their Lyα emission in the PTGS. A least-squares solution yields $\log W = 1.91 + (0.03 \pm 0.05)\ (z - 3.36)$, showing that there is no significant variation of the equivalent width with redshift. The line corresponds to the limiting *observed* equivalent width of 50 Å of the grism survey.

The resulting equivalent widths are given in Table 1 and their distribution shown in Fig. 1(c). The equivalent widths are plotted versus the redshift in Fig. 2. A least-squares solution yields $\log W = 1.91 + (0.03 \pm 0.05)\ (z - 3.36)$, showing that the Ly$\alpha$ equivalent width for quasars selected by their Lyα emission does not vary significantly with redshift. This result is surprising, since the appearance of the Lyα profile of most high redshift quasars suggests that the blue side of the line suffers absorption. The line in Fig. 2 corresponds to the cutoff of 50 Å in the observed equivalent widths. We see no concentration of objects near the cutoff line. We conclude that, unless there exists a large population of quasars with very weak Lyα emission, the loss of objects in the sample due to the cutoff in equivalent width is negligible.

Finally, we will find it useful to have the relation between the absolute magnitude, the line luminosity and the equivalent width. By combining Eqs. (13) and (15), we can express M_B as

$$M_B = 2.5\log W_0 - 2.5\log f_{Ly\alpha} - 5\log A(z) + 1.395\alpha - 61.60, \quad (16)$$

or, introducing the Lyα line luminosity from Eq. (5),

$$M_B = 2.5\log W_0 - 2.5\log L_{Ly\alpha} + 1.395\alpha + 82.48. \quad (17)$$

This equation allows one to convert the Lyα luminosity function into an M_B luminosity function. For a derivation of the appropriate value of the rest frame equivalent width W_0 to be used for the conversion; see Sec. 3.

3. THE RELATION BETWEEN LINE AND CONTINUUM LUMINOSITY FUNCTIONS

Since most studies of the luminosity function of quasars at lower redshifts express the results as a function of continuum luminosity, usually M_B, it is necessary to consider the relation between the line luminosity function and the continuum luminosity function.

The problem of converting one luminosity function into the other is closely related to that of relating source counts in different frequency bands. This is especially appropriate for our case, because we derive the line luminosity function in different redshift bands from the counts of quasars down to the line flux limit appropriate to that redshift. The relation between source counts in different frequency bands is of importance in radio astronomy (cf. Kellermann 1964), in galaxy counts, in galactic structure studies, etc.

As an example in galactic studies, counts of stars as a function of apparent magnitude may be available for blue and red magnitudes. It is often stated that the blue counts are "biased" toward blue, hot stars, and that the red counts are biased toward cool stars. It is more instructive to consider that these counts are integrals of bivariate counts of blue and red magnitudes. Clearly, blue counts and red counts cannot be exactly related, since the objects counted are not identical. But we can derive a statistical relation by determining for what difference between blue and red magnitude (i.e., for what effective color) the observed blue counts and red counts at some given magnitude are equal. Our derivation of the conversion of a line luminosity function into a continuum luminosity function given below is based on this concept.

Let us represent the line luminosity by an absolute magnitude M_L, and the continuum luminosity per unit bandwidth by M_B. The "color" $C=M_B-M_L$ characterizes the line-to-continuum ratio. The color distribution at given L is denoted as $f_L(C)$. We assume that the distribution $f_L(C)$ is independent of the line luminosity L. Let the bivariate luminosity function be $\Psi(M_L,M_B)dM_L\,dM_B$. The luminosity functions $\Phi(M_L)$ and $\Phi(M_B)$ are obtained by integrating the bivariate luminosity function over M_B and M_L, respectively.

We assume that the luminosity function is a power law of the line luminosity, or an exponential function of M_L. In that case,

$$\Psi(M_L,M_B)dM_L\,dM_B=\text{const}\ e^{\beta M_L}f_L(C)dM_L\,dM_B. \tag{18}$$

This can also be written as

$$\Psi(M_L,M_B)dM_L\,dM_B=\text{const}\ e^{\beta M_B}f_B(C)dM_L\,dM_B, \tag{19}$$

where the color distribution $f_B(C)$ at given B is

$$f_B(C)=f_L(C)e^{-\beta C}, \tag{20}$$

which is equivalent to the relation between radio source counts at different frequencies derived by Kellermann (1964). This equation relates the color distribution of quasars selected by M_L to that of quasars selected by M_B. We had assumed that $f_L(C)$ was independent of M_L. If this is the case, we now see from Eq. (20) that $f_B(C)$ is independent of M_B, i.e., *there is symmetry between line luminosity and continuum luminosity.*

By integrating Eq. (18) over all colors C at fixed M_L, we obtain the luminosity function of M_L,

$$\Phi(M_L)=\text{const}\ e^{\beta M_L}\int_{-\infty}^{+\infty}f_L(C)dC. \tag{21}$$

Similarly, by integration of Eq. (19),

$$\Phi(M_B)=\text{const}\ e^{\beta M_B}\int_{-\infty}^{+\infty}f_B(C)dC. \tag{22}$$

As discussed above, we now *define* the equivalence of M_L and M_B by the requirement that $\Phi(M_L)=\Phi(M_B)$. The corresponding difference M_B-M_L or effective color $C_{\rm eff}$ is given by

$$e^{-\beta C_{\rm eff}}=\int_{-\infty}^{+\infty}e^{-\beta C}f_L(C)dC\ \Big/\int_{-\infty}^{+\infty}f_L(C)dC \tag{23}$$

or

$$e^{-\beta C_{\rm eff}}=\langle e^{-\beta C}\rangle_L, \tag{24}$$

where the subscript L indicates that the average is taken using the line selected color distribution $f_L(C)$.

We can rephrase the result in terms of luminosities, with a luminosity function that is a power law of luminosity, equivalent to an exponential function of magnitude. The effective color $C_{\rm eff}$ corresponds to a ratio of L and B luminosities, which translates into an effective equivalent width $W_{0,\rm eff}$. If the luminosity function is

$$\Phi(L)d\,\ln L=\text{const}\ L^{\gamma}\,d\ln L, \tag{25}$$

and if $f_L(W_0)$ and $f_B(W_0)$ are the distributions of equivalent widths per unit log L, then from Eq. (20) the relation between these two distributions is

$$f_B(W_0)=f_L(W_0)W_0^{\gamma}. \tag{26}$$

The effective equivalent width $W_{0,\rm eff}$ for conversion of the line luminosity function into the continuum luminosity function [cf. Eq. (24)] is given by

$$W_{0,\rm eff}^{\gamma}=\langle W_0^{\gamma}\rangle_L, \tag{27}$$

where the subscript L indicates that the average is to be taken using equivalent widths from a sample selected by line emission.

Based on the rest frame equivalent widths W_0 derived in Sec. *2.3* and listed in Table 1 and the value of γ [cf. Eq. (35)], we find

$$W_{0,\rm eff}=67.6\pm1.0\ \text{Å}, \tag{28}$$

which applied to Eq. (17) with $\alpha=-0.5$ yields

$$\langle M_B\rangle_L=86.36-2.5\langle\log L_{\rm Ly\alpha}\rangle, \tag{29}$$

The subscript L again signifies that the average refers to a sample selected by line emission.

3.1 An Illustration

We present a brief illustration of the conversion of the line luminosity function into the M_B continuum luminosity func-

TABLE 2. An example of a bivariate line-continuum luminosity function.

log L	44.48	44.74	45.00	45.26	45.52	
M_B						W_0 = 33 Å
28.22					1.0	W_0 = 60 Å
27.57				2.9	3.7	W_0 = 110 Å
26.92			9.0	11.4	4.2	W_0 = 200 Å
26.27		27.6	35.0	12.7	0.7	
25.62	84.5	107.2	39.0	2.3		
24.97	328.5	119.5	7.0			
24.32	366.0	21.4				
23.67	65.7					

tion. In order to make the illustration simple, we put the equivalent widths W_0 given in Table 1 in four logarithmic bins of width 0.26 centered on $\log W_0$ values of 1.52, 1.78, 2.04, and 2.30, containing 9, 35, 39, and 7 objects, respectively. Since in writing Eq. (18), we assumed that the distribution of colors (here equivalent widths) was independent of luminosity, we assume for this illustration that all these objects have a line luminosity $\log L = 45.00$; cf. the fourth column of Table 2.

We can now derive all the remaining entries in Table 2. The M_B values given in the first column are obtained from Eq. (17). Given the slope γ of the luminosity function [cf. Eqs. (33) and (35)], the counts change by a factor of 3.06 per interval along diagonals of constant equivalent width. We now ask the question: Given that at $\log L = 45.00$ we have 90 objects, at what value of M_B is this the case? We find by interpolation in the horizontal sums that this happens at $M_B = -26.17$. According to Eq. (29) this should be -26.14, the difference being due to the effect of the wide bins in this example.

The vertical distribution of the equivalent widths in each column of Table 2 corresponds to the observed distribution on the PTGS. The horizontal distribution in each row is representative of the equivalent width distribution we would expect for continuum-selected quasars. In particular, the horizontal distribution of $\log W_0$ at $M_B = -26.14$ is 33, 41, 15, and 1, in contrast to the vertical distribution at $\log L = 45.00$ of 9, 35, 39, and 7. As we would expect, quasars chosen by their continuum flux have smaller Lyα equivalent widths (we predict a median of 56 Å) than those chosen by line flux (for which the observed median is 81 Å). This is precisely the effect discussed for colors of stars in the beginning of Sec. 3. The bivariate distribution of Table 2 allows quantitative discussion of the relation between samples chosen by line or by continuum flux.

4. DERIVATION OF THE LUMINOSITY FUNCTION

In this section we derive the Lyα luminosity function in the redshift range 2.7–4.7. We also derive the equivalent M_B continuum luminosity function to allow a comparison with luminosity functions derived at lower redshifts.

4.1 Derivation of z_{min}, z_{max}, and the V/V_{max} Test

In order to carry out tests for the uniformity of the space distribution of the objects in the survey, we need to determine the minimum and maximum redshifts at which each individual quasar can be observed in the PTGS. The procedure is illustrated in Fig. 3, in which we show a plot of the redshift z versus the detected line flux $f_{\rm det}$ for the 32 quasars detected in one of the six surveys of the PTGS. The curved envelope on the right-hand side of the figure corresponds to the limiting line flux $f_{\rm lim}(\lambda)$ of the QR survey (cf. Table 3 and Fig. 6 of Paper III), at a wavelength $\lambda = 1216\ (1+z)$ Å.

Consider a given quasar of line luminosity $L_{\rm Ly\alpha}$, rest frame linewidth $w_{\rm rest}$ and rest frame equivalent width $E_{\rm rest}$. If this object is observed at any redshift z, the detected line flux will be $L_{\rm Ly\alpha} R_w / 4\pi (A(z) c/H_0)^2$, where $w = w_{\rm rest}\ (1+z)$ is the linewidth used to read R_w from Table 4 in Paper III. By iteration, we can find the smallest and largest values of the redshift, $z_{\rm min}$ and $z_{\rm max}$, respectively, at which the detected line flux would equal the limiting line flux, or at which the wavelength limits of the grism survey are reached. Figure 3 shows the locus of one of the quasars as its redshift is varied between $z_{\rm min}$ and $z_{\rm max}$.

We are now able to carry out the $V/V_{\rm max}$ test (Schmidt 1968). We adapt the test to the existence of a nonzero minimum redshift, so

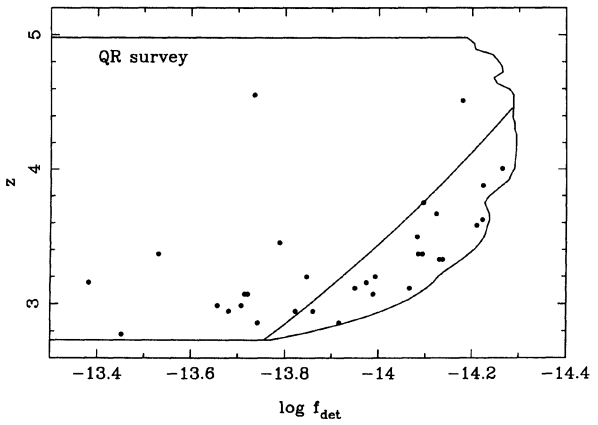

FIG. 3. Redshift vs detected Lyα line flux for the 32 quasars detected by their Lyα emission in a subsurvey ("QR") of the PTGS. The envelope outlines the limiting detected flux (on the right side, as a function of wavelength) and the limiting redshifts (top and bottom) of the QR subsurvey. The curved line delineates the path described by one of the quasars as the object is hypothetically moved along the line of sight until it disappears from the survey.

$$\frac{V}{V_{\max}}=\frac{V(z)-V(z_{\min})}{V(z_{\max})-V(z_{\min})}, \tag{30}$$

where $V(z)$ is derived from Eq. (2). We find for the entire sample of 90 quasars detected by their Lyα emission,

$$\langle V/V_{\max}\rangle=0.385\pm0.028, \tag{31}$$

where the given mean error is based on the rms deviation of the individual $V/V_{\max}$ values from the average.

Alternatively, we use the extension of the test proposed by Avni & Bahcall (1980) for surveys in which the limiting sensitivity is a function of direction. They define V_a as the total accessible volume within which a given quasar is observable in the survey. The volume V_e is that part of the accessible volume that is at a redshift smaller than the quasar's redshift z. To apply the test, we derive limiting redshifts $z_{\min}$ and $z_{\max}$ for each Lyα quasar in each of the six survey fields. We derive V_e and V_a taking into account the effective areas of each of these fields (cf. Table 2 in Paper III).

Our sample of 90 quasars detected by their Lyα emission yields

$$\langle V_e/V_a\rangle=0.377\pm0.026. \tag{32}$$

This value agrees within the statistical error with that from the $V/V_{\max}$ determination. The two values are more than 4σ below the value 0.50 expected for a uniform space distribution, showing that the comoving space density at given luminosity must decrease with increasing redshift.

If instead of the value for the deceleration constant $q_0=0.5$ adopted in this paper, we use $q_0=0.0$, then the $V/V_{\max}$ test yields $V_e/V_a=0.413\pm0.028$. In this case the significance of the decline in the comoving space density is reduced to a 3σ effect.

TABLE 3. Space density vs redshift.

z	$\langle z\rangle$	$n_{\rm pred}$	$n_{\rm obs}$	$\rho(z, M_B<-26)$ (Gpc^{-3})
< 3.22	2.98	43.6	43	147 ± 22
3.22 – 3.73	3.44	30.0	32	101 ± 18
3.73 – 4.24	3.95	11.8	10	48 ± 14
> 4.24	4.49	4.6	5	36 ± 17

4.2 The Shape of The Luminosity Function

We assume that the luminosity function is a power law of the line luminosity,

$$\Phi(L)d\ln L=\text{const}\,L^{\gamma}\,d\ln L. \tag{33}$$

Since the range of Lyα line luminosities among the 90 objects is only a factor of 10, it is unlikely that we can in fact find a significant deviation from the power law representation.

The fluxes $f_{\rm Ly\alpha,det}$ of quasars at given redshift z represent the luminosity function and therefore exhibit the same power law. It is easily shown that for the power law distribution given in Eq. (33), the average value of $\ln L$ above a limiting value $\ln L_1$ equals $\ln L_1-1/\gamma$. The corresponding relation for the fluxes $f_{\rm Ly\alpha,det}$ down to a limiting flux $f_{\rm lim}$ allows the derivation of γ as

$$\gamma=-\langle\ln(f_{\rm Ly\alpha,det}/f_{\rm lim})\rangle^{-1}. \tag{34}$$

From the line fluxes for the 90 quasars, together with the limiting fluxes given in Table 3 of Paper III we find

$$\gamma=-1.87\pm0.15, \tag{35}$$

corresponding to a factor of 5.6 per magnitude. The median redshift of the sample is 3.25. For $z<3.25$ we find $\gamma=-1.80$, while for $z>3.25$ $\gamma=-1.95$, i.e., there is no significant dependence of the slope on redshift. We can also derive the slope for a subset of the sample that is more luminous by increasing the limiting line fluxes $f_{\rm lim}$ by a fixed amount. This subset will have higher luminosities, but, as in the original sample, there is not a well-defined luminosity limit. To create the subset, the limiting line fluxes $f_{\rm lim}$ are increased by an amount, such that half of the original sample survives. For this subset, we find $\gamma=-2.24\pm0.25$. The difference with the slope from the full set is marginally significant.

4.3 Derivation of the Comoving Density Variation

Before we derive the comoving density at given luminosity as a function of redshift, we investigate the systematic effect on our sample of the rms errors in the line fluxes. Since the power law slope is negative [see Eq. (35)], there are more quasars with line fluxes below our survey than there are above the limit. As a consequence, random errors in the line fluxes will cause more objects to be added to our sample than be lost, the so-called Eddington effect. Assuming that the error distribution is Gaussian with dispersion σ, the correction to the observed counts is $-(\sigma^2/2)(d^2n/dm^2)$, where $n=n(m)$ represents the differential counts (Eddington 1940). At a given redshift, objects in our sample have a power law distribution [cf. Eq. (33)] of the line flux, to a limiting signal-to-noise ratio of 7 or 6.5, i.e., $\sigma\sim0.15$ mag. The Eddington

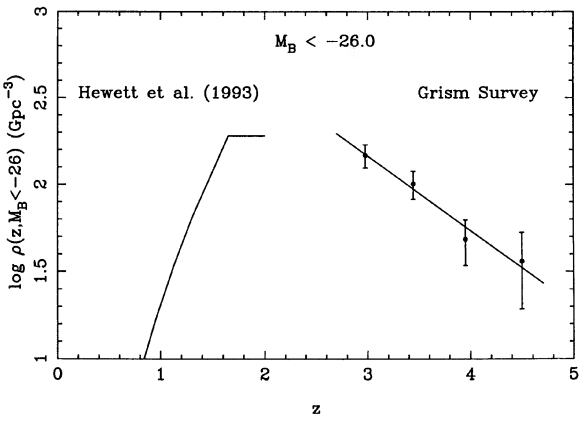

FIG. 4. Comoving space density of quasars with $M_B<-26$ versus redshift z. The line for $z<2$ is based on the luminosity functions of Hewett *et al.* (1993). The four points represent the results from the grism survey. The line is a best-fit exponential density law [cf. Eq. (36)].

correction to the counts is -3% at the flux limit, less for brighter objects. The correction for the sample as a whole is probably around -2%. As this is much smaller than the RMS sample errors, we have not applied any correction.

Our goal is to derive the variation with redshift of the quasar comoving space density above a given luminosity. We have already adopted a power law for the luminosity function at given redshift [cf. Eq. (33)]. We now assume that the density variation at given luminosity is a power law of the redshift. Starting with an estimated value of the slope of the density power law, we use the characterization of the PTGS given in this paper to derive an expected numbers of Lyα detected quasars in four redshift bins (see Table 3). Next we find the "observed" density above a given luminosity (we use $M_B<-26$) at a given $\langle z\rangle$ in each bin by multiplying the density given by the power law density function by the ratio of observed to predicted numbers in the redshift bin. A least squares solution of these densities versus the $\langle z\rangle$ values yields the slope of the density power law, which is used in the next iteration of the process. Expressed in terms of a cumulative luminosity function for absolute magnitude brighter than M_B in units of Gpc^{-3}, we find

$$\log \Phi(z,<M_B)=2.165-0.43(z-3)+0.748(M_B+26). \quad (36)$$

This representation of the luminosity function is only intended to cover the redshift range ($2.7<z<4.7$) and the range of absolute magnitudes ($-27.5<M_B<-25.5$) of the PTGS Lyα quasars. The formal mean error of the slope (0.43) is ± 0.04 but it is likely that (unknown) systematic errors dominate. With this slope, the comoving space density at given luminosity decreases by a factor of 2.7 per unit redshift. We give in Table 3, the comoving densities for $M_B<-26$ in four redshift bins. The values shown are those obtained from Eq. (36) at the given $\langle z\rangle$, multiplied by the ratio of observed overpredicted numbers in the redshift bin. They are illustrated in Fig. 4 together with the density law. Also shown in Fig. 4 is the comoving space density for $M_B<-26.0$ for $z<2$ based on Hewett *et al.* (1993) (see Sec. 5).

These results are based on a slope of the luminosity function of $\gamma=-1.87$ [Eq. (35)] and the corresponding rest frame Lyα equivalent width of 67.6 Å. The uncertainty in the value of γ is probably best characterized by the finding that the more luminous half of the quasar sample yields a value of $\gamma=-2.24$ (cf. the end of Sec. *4.2*). If we were to employ this value of γ for the whole sample, then the rest frame equivalent width changes to 65.2 Å and the densities given in Table 3 become 151, 101, 52, and 44, respectively. All the changes are at least a factor of 2 smaller than the rms errors of the densities given, showing that the uncertainty in the slope of the luminosity function has no substantial effect on the space density results.

In Sec. *3.4* of Paper III, we discussed the effect of the Lyα forest on the F555W image catalog which is the basis for inclusion in the PTGS. The question was whether the effect of the forest absorption could be so large that the image catalog for any of our observed quasars could be shallower than the grism survey. A quantitative evaluation showed no indication that any bias against the detection of Lyα emission lines had been introduced for redshifts below 4.4. At larger redshifts, a small correction to the flux limits given in Table 3 of Paper III may be required. Introduction of this correction, which is uncertain and which we have ignored, would increase the comoving space density for $z>4.24$ in Table 3 of this paper.

5. COMPARISON WITH OTHER SURVEYS

Luminosity functions of quasars at high redshifts are usually compared to those of redshift 2. Until recently, the $z=2$ luminosity functions of Boyle *et al.* (1988) or Boyle (1991) were used for this purpose. Hewett *et al.* (1993) discuss the results of the LBQS and show among other things that the observed number of quasars in the redshift interval 1.5–2.0 is significantly smaller than that predicted by the Boyle models. Hewett *et al.* illustrated the size of the changes by an *ad hoc* modification of the parameters of the two power-law representation of the luminosity function as a function of redshift. Their parameters for the redshift interval 1.5–2.0 were identical to those used by Boyle (1991), except that the luminosity evolution was halted at $z=1.65$. As a consequence, the Hewett *et al.* $z=2$ luminosity function is a factor of 2–3 lower than the Boyle function. We have used this parametrization to derive the $z=2$ luminosity function. Since the Hewett luminosity function is in terms of M_{B_J}, we convert it to M_B by a correction of $+0.07$ mag, based on transformations given in Foltz *et al.* (1989).

From our own and two other studies of high redshift quasars discussed below, we derive the $z=4$ luminosity function, in order to compare the surveys among themselves and to the $z=2$ luminosity function.

5.1 The UK Schmidt Survey

The UK Schmidt Survey (Warren *et al.* 1994) is a six-band photographic color survey effectively covering 43 deg^2

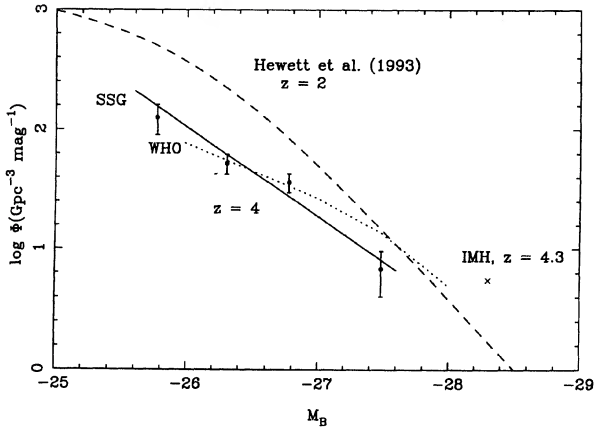

FIG. 5. Differential luminosity functions at $z=2$ and $z\sim4$. The labels indicate results from the present paper (SSG), Warren *et al.* (1993) (WHO), and Irwin *et al.* (1991) (IMH). The four points represent the luminosity function from the grism survey, based on the density law given in Eq. (36); see the text.

to a limiting magnitude of 20. Candidates were selected from the photometric catalog of stellar images by identifying objects that lie away from the locus of common stars in six-dimensional parameter space defined by the six magnitudes. The sample includes 86 quasars with $2.2<z<4.5$, including 8 with $z>3.5$ and 1 with $z>4.0$.

Warren *et al.* present a very detailed and thorough derivation of the detection probability as a function of absolute magnitude M and redshift as derived from statistical considerations including the spectral energy distribution, the emission line strength, the probability of absorption by Lyα clouds and Lyman-limit systems, and quasar variability. Many of the quasars in the sample lie in areas of the (M,z) diagram where the detection probability ranges from 20%–60%.

With only eight quasars with $z>3.5$, and large incompleteness corrections, the luminosity function at large redshifts is poorly established. Warren *et al.* used the luminosity function for $3.0<z<3.5$ to derive the expected number for $3.5<z<4.5$ on the assumption that there is no evolution between the two redshift intervals. The expected number was 52, compared to 8 observed. Following Warren *et al.* [1994, Fig. 5(b)], we divide their luminosity function for $3.0<z<3.5$ by a factor of 6.5 to represent the luminosity function at $z=4$. To allow comparison with other work (cf. Fig. 5), we convert their $M_C(1216)$ absolute magnitudes into M_B through $M_B-M_C(1216)=-0.60$ (Warren 1994). This is based on a spectral index $\alpha=-0.5$ [cf. Eq. (9)] for the continuum energy distribution that we have used throughout. We also rescale their results, based on $H_0=75$ km s^{-1} Mpc^{-1}, to our assumed value of $H_0=50$ km s^{-1} Mpc^{-1}.

5.2 The UK Schmidt APM Survey

The UK Schmidt APM Survey (Irwin *et al.* 1991) is a three-color band photographic survey covering an effective area of 1600 deg^2 to $R=19$. Candidate quasars were primarily selected by $B-R$ color. The sample contains 20 quasars with $z>4.0$. No details about the photometric calibration and the derivation of the luminosity function are available. Irwin *et al.* state that the comoving space density for $M_B<-27.8$ at $z=4.3$ is 6 Gpc^{-3}. We represent this result in terms of a differential luminosity function at $z=4.3$ by an entry in Fig. 5 of 5.5 Gpc^{-3} mag^{-1} at $M_B=-28.3$.

5.3 Comparison of Results

We show in Fig. 5 the observed portions of the differential luminosity functions at $z\approx4$ from the three high redshift studies, together with the Hewett *et al.* $z=2$ function. For our survey, we have plotted the adopted power law with slope -1.87 [cf. Eq. (36)]. In addition we show four points based on the assumption that $\log\rho(z,M_B<-26)\sim-0.43(z-3)$. [This is the complementary approach to that taken in this paper, i.e., here we assume a density law and derive the luminosity law, while elsewhere in the paper we adopt the luminosity law; cf. Eq. (33) and derive the density law.]

Our luminosity function at $z=4$ is in close agreement with that by Warren *et al.* for $M_B\sim-26.5$, but is generally steeper than the latter. Judging by the four points representing the grism results, the difference in slope is hardly significant. The excellent agreement between our $z=4$ luminosity function and that by Warren *et al.* is remarkable, considering the very different methods employed.

At $M_B\sim-28$, the Irwin *et al.* result suggests positive evolution from $z=2$ to $z=4.3$. In order to evaluate whether the results of our grism survey disagree with those of Irwin *et al.*, we first use Eq. (36) and deduce that we would expect around one quasar with $M_B<-27.8$ with $z>3.7$ in the grism survey (actually, we observe none; see Fig. 1). If we now accommodate the Irwin *et al.* result at $z=4.3$ by allowing the slope of the luminosity function to evolve with redshift, such that it fits the PTGS results at lower luminosities and the Irwin point at $M_B\sim-28$ and $z=4.3$, then the predicted number of quasars with $M_B<-27.8$ and $z<3.7$ in the grism survey rises to around 3. Clearly, our grism survey is not critically sensitive to the quasars of higher luminosity contained in the Irwin *et al.* (1991) survey.

5.4 A Historical Note

As mentioned in the Introduction, our first transit survey [Schmidt *et al.* (1986b, Paper II] did not produce any quasars with redshifts $z>3$. With the luminosity function produced in this paper, we can check after the fact how many such quasars we could have expected to find. In particular, we use the luminosity function given in Eq. (36) converted [cf. Eq. (29)] to a Lyα line luminosity function. The limiting fluxes can be derived from Tables 4 and 5 in Paper II. We find that the transit survey described in the 1986 paper should have produced 3.4 quasars with $z>3$. Since the limiting line fluxes are typically two times larger than those in the PTGS at relevant wavelengths and since the luminosity function steepens for higher luminosities (cf. Sec. *4.2*), the predicted number is an upper limit. Considering the small number, we

conclude that the null result of Paper II is not inconsistent with the results from the present paper.

6. CONCLUSION

The detection criterion for the PTGS involves essentially the detection of an emission line as a point source on the grism exposures. Admittedly, the Lyα line is resolved and a second criterion involving a minimum equivalent width is employed, but the corrections for these two complications are small, and negligible, respectively. The well-defined wavelength-dependent flux limit leads to a sharp detection limit, witness the small size of the Eddington correction.

The price we pay for using the Lyα emission line as the detection signal is that we obtain properties as a function of Lyα line luminosity whereas most other studies are related to continuum luminosities such as M_B. Both types of fluxes vary with the inverse square of the luminosity distance, making them equally suitable for studies of the luminosity function. The conversion from one to the other type of luminosity function discussed in Sec. 3 is based on symmetry between the two. Once the physics of the continuum and line luminosities is well understood, there may be a basis for preference of one over the other. At the present time, we find at high redshifts the operational advantages of working with the Lyα emission line compelling.

The significance of our result that the comoving space density of quasars with $M_B < -26$ decreases with redshift for $z > 2.7$ is probably best expressed by the $V/V_{\max}$ test which produced a deviation from uniformity in excess of 4σ. The increase in comoving space density exhibited by the luminosity functions of Hewett *et al.* (1993) and the decrease seen in our grism results exhibited in Fig. 4 show that there was a maximum between redshifts 1.7 and 2.7. These redshifts correspond to cosmic epochs 3.0 and 1.9 billion years, respectively, following the Big Bang. Understanding a peak quasar activity around 2.5 billion years after the Big Bang will be a major challenge for theories concerned with the formation of galaxies, black holes, and quasars.

M.S. thanks S. J. Warren for discussions on the relationship between continuum and line surveys. This work was supported in part by the National Science Foundation Grants No. AST87-15508, No. AST91-08834, and No. AST94-15574 (M.S.) and No. AST91-00121 (J.E.G.), and NASA Contract No. NAG5-1618 (D.P.S.).

REFERENCES

Avni, Y., & Bahcall, J. N. 1980, ApJ, 235, 694
Boyle, B. J. 1991, in Texas/ESO-CERN Symposium on Relativistic Astrophysics, Cosmology and Fundamental Physics, edited by J. D. Barrow, L. Mestel, and P. A. Thomas (Ann. N.Y. Acad. of Sci. No. 647), 14
Boyle, B. J., Shanks, T., & Peterson, B. A. 1988, MNRAS, 235, 935
Crampton, D., Cowley, A. P., & Hartwick, F. D. A. 1987, ApJ, 314, 129
Eddington, A. S. 1940, MNRAS, 100, 354
Efstathiou, G., & Rees, M. J. 1988, MNRAS, 230, 5P
Foltz, C. B., Chaffee, F. H., Hewett, P. C., Anderson, S. F., & MacAlpine, G. M. 1989, AJ, 98, 1959
Haehnelt, M. G., & Rees, M. J. 1993, MNRAS, 263, 168
Hewett, P. C., Foltz, C. B., and Chaffee, F. H. 1993, ApJ, 406, L43
Irwin, M. J., McMahon, R. G., and Hazard, C. 1991, in The Space Distribution of Quasars, edited by D. Crampton (ASP, San Francisco), p. 117
Katz, N., Quinn, T., Bertschinger, E., & Gelb, J. M. 1994, MNRAS, 270, L71
Kellermann, K. I. 1964, ApJ, 140, 969
Loeb, A. 1993, ApJ, 403, 542
Morris, S. L., Weymann, R. J., Anderson, S. F., Hewett, P. C., Foltz, C. B., Chaffee, F. H., Francis, P. J., & MacAlpine, G. M. 1991, AJ, 102, 1627
Oke, J. B. 1974, ApJS, 27, 21
Osmer, P. S. 1980, ApJS, 42, 523
Osmer, P. S. 1982, ApJ, 253, 28
Schmidt, M. 1968, ApJ, 151, 393
Schmidt, M. 1970, ApJ, 162, 371
Schmidt, M., & Green, R. F. 1983, ApJ, 269, 352
Schmidt, M., Schneider, D. P., & Gunn, J. E. 1986a, ApJ, 306, 411 (Paper I)
Schmidt, M., Schneider, D. P., & Gunn, J. E. 1986b, ApJ, 310, 518 (Paper II)
Schmidt, M., Schneider, D. P., & Gunn, J. E. 1987a, ApJ, 316, L1
Schmidt, M., Schneider, D. P., & Gunn, J. E. 1987b, ApJ, 321, L7
Schneider, D. P., Schmidt, M., & Gunn, J. E. 1989a, AJ, 98, 1507
Schneider, D. P., Schmidt, M., & Gunn, J. E. 1989b, AJ, 98, 1951
Schneider, D. P., Schmidt, M., & Gunn, J. E. 1991, AJ, 101, 2004
Schneider, D. P., Schmidt, M., & Gunn, J. E. 1994, AJ, 107, 1245 (Paper III)
Smith, M. G. 1983, in Proceedings of the 24th Liege Colloquium, Quasars and Gravitational Lenses (Institut d'Astrophysique, Liege), p. 4
Turner, E. L. 1991, AJ, 101, 5
Warren, S. J. 1994, private communication
Warren, S. J., Hewett, P. C., & Osmer P. S. 1994, ApJ, 421, 412